A Multi-dimensional Two-Phase Eulerian Model for Sediment Transport — TwoPhaseEulerSedFoam (Version 1.0)

BY

ZHEN CHENG AND TIAN-JIAN HSU
CENTER FOR APPLIED COASTAL RESEARCH
UNIVERSITY OF DELAWARE

RESEARCH REPORT NO. CACR-14-08
AUGUST 2014

CENTER FOR APPLIED COASTAL RESEARCH

Ocean Engineering Laboratory
University of Delaware
Newark, Delaware 19716, USA

Acknowledgements

This study is supported by National Sceince Foundation (CMMI-1135026; OCE-1356855) and Office of Naval Research (N00014-14-1-0586, Littoral Geosciences and Optics Program). Numerical simulations are carried out on CHIMERA at the University of Delaware with funding supported by the National Science Foundation (CNS-0958512). Simulations also leverage computing resource provided by Extreme Science and Engineering Discovery Environment (XSEDE) (TG-OCE100015). We gratefully acknowledge developers involved in OpenFOAM, which is the foundation of the new solver twoPhaseEulerSedFoam presented in this report. Dr. Xiao Yu provided many useful suggestions during the model development.

Abstract

A multi-dimensional numerical model for sediment transport based on the two-phase flow formulation is developed. With closures of particle stresses and fluid-particle interaction, the model is able to resolve processes in the concentrated region of sediment transport and hence does not require conventional bedload/suspended load assumptions. The numerical model is developed in three spatial dimensions. However, in this version, the model is only validated for Reynolds-averaged two-dimensional vertical (2DV) formulation (with the $k - \epsilon$ closure for carrier flow turbulence) for sheet flow in steady and oscillatory flows. This numerical model is developed via the open-source CFD library of solvers, OpenFOAM and the new solver is called twoPhaseEulerSedFoam. This report is written as the documentation of the open-source solver twoPhaseEulerSedFoam and it includes the mathematical formulation, numerical methodology, model validation, installation procedures and model input/output.

Contents

List of Figures

List of Tables

1 Introduction

Numerical models for coastal morphological evolution (*Jacobsen et al.*, 2012; *Warner et al.*, 2008; *Lesser et al.*, 2004), scour (*Liu and Garcia*, 2008) and bedform dynamics (*Marieu et al.*, 2008; *Chou and Fringer*, 2010) typically split the total sediment transport into bedload and suspended load components. Invoking dilute flow assumptions, suspended load transport is resolved in order to capture resuspension, advection, and deposition driven by complex turbulent flows. However, the concentrated region of sediment transport near the bed, often referred to as the bedload, cannot be resolved in this type of models and semi-empirical parameterizations of bedload transport rate (*Ribberink*, 1998) and pickup flux (*Engelund and Fredsoe*, 1976; *van Rijn*, 1984) are used to complete the mathematical description. These semi-empirical parameterizations are often direct extension from simple flow conditions and hence many key assumptions are adopted (e.g., ignoring unsteadiness) when applied to coastal environments.

On the other hand, the two-phase flow approach can resolve concentrated region of sediment transport (see Figure 1) by including closures of particle stresses and fluid-particle interactions in the governing equations. In the past decades, several two-phase numerical models have been developed, where the sediment phase is modeled either with an Eulerian scheme (*Dong and Zhang*, 1999, 2002; *Hsu et al.*, 2004; *Li et al.*, 2008; *Amoudry and Liu*, 2009; *Bakhtyar et al.*, 2010) or a Lagrangian scheme (*Drake and Calantoni*, 2001). These two-phase models can resolve the full profiles of sediment transport without the need to divide the transport into bedload and suspended load components. Using a two-phase model, researchers can quantify the total transport load under waves driven by higher-order wave statistics (*Dong and Zhang*, 2002; *Hsu and Hanes*, 2004; *Calantoni and Puleo*, 2006; *Liu and Sato*, 2006), wave-induced boundary layer streaming (*Yu et al.*, 2010; *Kranenburg et al.*, 2014) and wave-breaking turbulence (*Scott et al.*, 2009). Two-phase models are also used to improve the parameterization of pickup flux in suspended load module under waves (*Amoudry and Liu*, 2010; *Yu et al.*, 2012).

Most of the existing two-phase models are based on the Reynolds-averaged approach and simplified into one-dimensional-vertical (1DV) formulation. 1DV models cannot capture the development of inhomogeneous flow features (e.g., bedforms), flow instabilities and scour (*Amoudry and Liu*, 2009). Hence, existing two-phase models are restricted to sheet flow applications where the ensemble-averaged flow field is more or less fully developed in the streamwise and spanwise directions. Moreover, 1DV model cannot resolve three-dimensional (3D) turbulence and turbulence-sediment interaction. For example, in the 1DV model of *Kranenburg et al.* (2014), they showed that model results are sensi-

tive to the parameterization of turbulence-sediment interaction (damping of carrier flow turbulence due to the presence of sediment). By invoking fine sediment assumption to further simplify the two-phase equations, *Penko et al.* (2010) developed a 3D mixture model that is able to resolve turbulence over evolving sand ripples. Similar turbulence-resolving simulation model is developed by *Ozdemir et al.* (2010) to study the transition of flow modes of fine sediment in the wave boundary layer due to turbulence-sediment interaction. Although the mixture approach is further simplified from the complete two-phase flow equations (*Balachandar and Eaton*, 2010), these two studies clearly demonstrate the importance of resolving flow turbulence in sediment transport. Hence, we are motivated to develop a three-dimensional two-phase model for sediment transport by extending the existing 1DV modeling strategy.

We have recently developed a 3D model for sediment transport that solves the complete Eulerian two-phase equations and this report is intended to describe this new model. Although the numerical model is written in 3D, the current version of the model has only been validated with 2DV Reynolds-averaged mode, which is presented later. The mathematical formulation of the two-phase model developed here is similar to *Hsu et al.* (2004) (see also *Yu et al.* (2010, 2012)), where the Eulerian two-phase flow equations for fluid and sediment phases are solved. In the 2DV Reynolds-averaged formulation, we adopt the $k-\epsilon$ closure for carrier flow turbulence, which includes semi-empirical terms to represent the damping of flow turbulence due to sediment. The kinetic theory of *Lun et al.* (1984) is used for the closure of collisional particle stresses, and simple phenomenological closures (*Johnson and Jackson*, 1987; *Srivastava and Sundaresan*, 2003) are used for particle stresses in the layer of enduring contact. The mathematical formulation is solved numerically using the open-source CFD library of solvers, OpenFOAM. OpenFOAM includes several multiphase flow modeling capabilities, such as bubbly flow (*Rusche*, 2002). Specifically, a two-phase flow solver in OpenFOAM called, twoPhaseEulerFoam (*Rusche*, 2002; *Weller*, 2002; *Peltola*, 2009) is adopted as the baseline. In the past several years, we devoted a considerable amount of efforts to improve the numerical stability of the solver and to include additional capabilities needed for coastal sediment transport applications. This document is intended to report the mathematical formulation of the Eulerian two-phase model for sediment transport, the numerical methodology and new modifications made to the twoPhaseEulerFoam solver provided by OpenFOAM. This new sediment transport model is named twoPhaseEulerSedFoam.

Scientific progresses made in modeling coastal processes have been facilitated by the development of open-source coastal modeling systems such as ROMS (*Warner et al.*, 2008), DELFT3D (*Lesser et al.*, 2004), NearCom-TVD (*Chen et al.*, 2014), and many

others. These models allow field experimentalists to utilize sophisticated models as an analytical tool to help to interpret observational data. Moreover, these open-source coastal models also help theoreticians and small-scale modelers to test their hypotheses and new parameterizations of processes that cannot be resolved in these large-scale models. However, for researchers studying small-scale, intra-wave coastal processes, such open-source numerical model is lacking. Since the introduction of the CFD open-open source library of solvers, OpenFOAM, developing open-source numerical modeling tool for small-scale coastal applications has become much more convenient (e.g., see nearshore wave modeling application by *Jacobsen et al.* (2012); *Higuera et al.* (2013)). To make a leap to improve our capability in modeling critical sediment transport mechanisms, open-source numerical modeling tools for small-scale processes must be made available to the research community. This work is intended to address this critical research infrastructure issue in the context of non-cohesive sediment.

This report is written as the documentation of the twoPhaseEulerSedFoam solver. The remaining of this report is organized as follow. The mathematical formulation of the two-phase sediment transport model is discussed in Section 2. The numerical methodology is discussed in Section 3 with additional references associated with the original OpenFOAM library of solvers provided. Model validation for the present 2DV Reynolds-averaged formulation is presented in Section 4. Conclusion and future work is discussed in Section 5. The Appendix include procedures for the installation of the numerical model and model input/output.

2 Model Formulations

Drew (1983) has derived the Eulerian two-phase flow equations via averaging over carrier fluid and dispersed particles. The resulting governing equations for Eulerian two-phase flow can be considered as the counterpart of the clear fluid Navier-Stokes equations. Hence, in order to apply these equations to turbulent flow without resolving all the scales of turbulence (larger than the grain scale), additional turbulence averaging or filtering is necessary. *Hsu et al.* (2003, 2004) has developed an Eulerian turbulence-averaged two-phase model to study sediment transport in sheet flow condition. In the present study, we extend the two-phase flow formulation similar to *Hsu et al.* (2004) for multi-dimensional sediment transport.

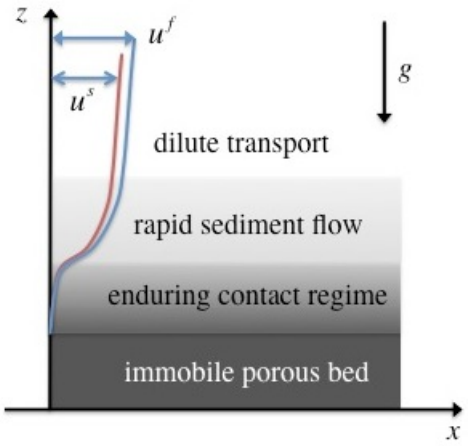

Figure 1: Schematic plot of sheet flow sediment transport with several vertical layers signifying the transport dominated by different mechanisms

Figure 1 shows a schematic plot of sheet flow sediment transport with vertical layers identified based on the dominant mechanisms. With the four-way coupled two-phase flow formulation along with appropriate closure models, the resulting model can resolve the full dynamics of sediment transport from the (porous) immobile bed, to the highly concentrated regions of transport dominated by enduring contact forces, to less dense region dominated by particle collision and turbulent suspension, and to the dilute suspended load region driven solely by flow turbulence. Particularly, the concentrated regions of sediment transport can be resolved by including closures of particle stresses and fluid-particle interactions in the governing equations. Hence, using the two-phase modeling approach for sediment transport, the resulting model does not require bedload/suspended load assumptions, commonly adopted by the single-phase flow approach. More details of this

modeling approach are discussed next.

2.1 Governing Equations

Although the present numerical model developed via the OpenFOAM numerical framework is naturally three-dimensional, the present model is only validated with turbulence-averaged two-dimensional vertical (2DV) formulation. Therefore, the governing equations and closures discussed in this version (twoPhaseEulerSedFoam version 1) will be based on the turbulence-averaged formulation. Assuming that there is no mass transfer between the two phases, the mass conservation equations for fluid phase and sediment phase can be written as:

$$\frac{\partial(1-\phi)}{\partial t}+\frac{\partial(1-\phi)u_i^f}{\partial x_i}=0 \tag{1}$$

$$\frac{\partial\phi}{\partial t}+\frac{\partial\phi u_i^s}{\partial x_i}=0 \tag{2}$$

where ϕ is the sediment volumetric concentration, u_i^f, u_i^s are i component of fluid and sediment phase velocities, respectively, and $i=1,2,3$ represents streamwise, spanwise and vertical components. The momentum equations for fluid and particle phases can be written as:

$$\begin{aligned}\frac{\partial\rho^f(1-\phi)u_i^f}{\partial t}+\frac{\partial\rho^f(1-\phi)u_i^fu_j^f}{\partial x_j}=&-\frac{\partial(1-\phi)p^f}{\partial x_i}+\frac{\partial(1-\phi)\tau_{ij}^f}{\partial x_j}\\&+\rho^f(1-\phi)g\delta_{i3}+M_i^{fs}\end{aligned} \tag{3}$$

$$\frac{\partial\rho^s\phi u_i^s}{\partial t}+\frac{\partial\rho^s\phi u_i^su_j^s}{\partial x_j}=-\frac{\partial\phi p^f}{\partial x_i}-\frac{\partial p^s}{\partial x_i}+\frac{\partial\tau_{ij}^s}{\partial x_j}+\rho^s\phi g\delta_{i3}+M_i^{sf} \tag{4}$$

where ρ^f, ρ^s are fluid and sediment density, respectively, g_i is the gravitational acceleration, p^f is the fluid pressure and τ_{ij}^f is the fluid shear stress, which includes fluid viscous stress and stresses associated with turbulence. Particle pressure p^s and particle stress τ_{ij}^s are calculated from kinetic theory of granular flow and phenomenological closure of frictional contact stresses. M_i^{fs} and M_i^{sf} represent the inter-phase momentum transfer between fluid phase and particle phase, and $M_i^{fs}=-M_i^{sf}$. Closures of the momentum transfer term and the stress terms for sediment transport are discussed next.

2.2 Inter-phase Momentum Transfer

In this framework of Eulerian two-phase flow formulation, both fluid and sediment phase are considered as continuum, and the momentum of these two phases are coupled through the inter-phase momentum transfer terms. The interaction between fluid phase and particle phase includes the drag force, the added mass force, the Basset force, the lift force (*Maxey and Riley*, 1983) and the effect of turbulence fluctuations on the effective momentum transfer. Typically, the drag force dominates in many sediment transport applications, and hence for simplicity we neglect the other terms such as lift force, added mass force and Basset force. In this version, the momentum exchange has the following form:

$$M_i^{fs} = -M_i^{sf} = -\phi\beta(u_i^f - u_i^s) - \beta\overline{\phi\Delta u_i^f} + p^f\frac{\partial(1-\phi)}{\partial x_i} \tag{5}$$

The last term on the right-hand-side (RHS) of equation (5) is the inter-phase pressure correction term, and the first two terms are due to drag force. The first term on the RHS of equation (5) represents averaged drag force due to mean relative velocity between fluid and particle phases, and the second term is the correlation term of sediment concentration and large-scale (larger than grain scale) fluid velocity fluctuations, often called turbulent suspension. The turbulent suspension terms is obtained from the Reynolds averaging (denoted as overbar), and can be modeled using gradient transport assumption (*McTigue*, 1981):

$$\overline{\phi\Delta u_i^f} = -\frac{\nu^{ft}}{\sigma_c}\frac{\partial\phi}{\partial x_i} \tag{6}$$

where ν^{ft} is the turbulent viscosity to be calculated with a turbulence closure and σ_c is the Schmidt number (see Table 1). For the closure of β, we adopt that suggested by *Ding and Gidaspow* (1990), who combined *Ergun* (1952) for dense sediment concentration ($\phi \geq 0.2$) and *Wen and Yu* (1966) for lower sediment concentration ($\phi < 0.2$):

$$\beta = \begin{cases} \frac{150\phi\nu^f\rho^f}{(1-\phi)d^2} + \frac{1.75\rho^f|u^f-u^s|}{d}, \phi \geq 0.2 \\ \frac{0.75C_d\rho^f|u^f-u^s|(1-\phi)^{-1.65}}{d}, \phi < 0.2 \end{cases} \tag{7}$$

where d is the sediment diameter, and C_d is expressed as:

$$C_d = \begin{cases} \frac{24(1+0.15Re_p^{0.687})}{Re_p}, Re_p \leq 1000 \\ 0.44, Re_p > 1000 \end{cases} \tag{8}$$

in which, $Re_p = (1-\phi)|u^f - u^s|d/\nu^f$ is the particle Reynolds number, and ν^f is the fluid molecular viscosity.

2.3 Fluid Turbulence Model

Because the present model equations are obtained by averaging over turbulence, the stresses are consisted of a large-scale component R_{ij}^{ft} (similar to Reynolds stress) and a small-scale stress r_{ij}^{f}, which includes the viscous stress and an additional fluid stress at grain scale (e.g., turbulence generated around individual particles). In the present study, stress associated with grain scale turbulence is neglected. Thus, the total fluid stress is written as:

$$\tau_{ij}^{f} = R_{ij}^{ft} + r_{ij}^{f} = \rho^{f}\big[\nu^{eff}\big(\frac{\partial u_i^f}{\partial x_j} + \frac{\partial u_j^f}{\partial x_i}\big) - \frac{2}{3}\nu^{eff}\frac{\partial u_k^f}{\partial x_k}\delta_{ij} - \frac{2}{3}k^f\delta_{ij}\big] \tag{9}$$

where k^f is the turbulent kinetic energy, and $\nu^{eff} = \nu^f + \nu^{ft}$ is the fluid effective viscosity. A modified $k-\epsilon$ model (***Hsu et al.***, 2004; ***Yu et al.***, 2010) is proposed to model the fluid turbulence:

$$\begin{aligned}\frac{\partial k^f}{\partial t} + u_j^f\frac{\partial k^f}{\partial x_j} = \frac{R_{ij}^{ft}}{\rho^f}\frac{\partial u_i^f}{\partial x_j} + \frac{\partial}{\partial x_j}\big[\big(\nu^f + \frac{\nu^{ft}}{\sigma_k}\big)\frac{\partial k^f}{\partial x_j}\big] - \epsilon^f - \frac{2\beta(1-\alpha)\phi k^f}{\rho^f(1-\phi)} \\ -\frac{1}{(1-\phi)}\frac{\nu^{ft}}{\sigma_c}\frac{\partial\phi}{\partial x_j}(s-1)g\delta_{j3}\end{aligned} \tag{10}$$

The balance equation for the rate of turbulent energy dissipation ϵ^f is assumed to be similar to that of clear fluid, except for the extra dissipation mechanism due to particle phase:

$$\begin{aligned}\frac{\partial \epsilon^f}{\partial t} + u_j^f\frac{\partial \epsilon^f}{\partial x_j} = C_{1\epsilon}\frac{\epsilon^f}{k^f}\frac{R_{ij}^{ft}}{\rho^f}\frac{\partial u_i^f}{\partial x_j} + \frac{\partial}{\partial x_j}\big[\big(\nu^f + \frac{\nu^{ft}}{\sigma_\epsilon}\big)\frac{\partial \epsilon^f}{\partial x_j}\big] - C_{2\epsilon}\frac{\epsilon^f}{k^f}\epsilon^f \\ -C_{3\epsilon}\frac{\epsilon^f}{k^f}\frac{2\beta(1-\alpha)\phi k^f}{\rho^f(1-\phi)} - C_{4\epsilon}\frac{\epsilon^f}{k^f}\frac{1}{(1-\phi)}\frac{\nu^{ft}}{\sigma_c}\frac{\partial\phi}{\partial x_j}(s-1)g\delta_{j3}\end{aligned} \tag{11}$$

where the parameter α is proposed to characterize the degree of particles following the fluid velocity fluctuations and it can be quantified by the Stokes number St (***Benavides and van Wachem***, 2008):

$$St = \frac{\tau_p}{\tau_l} \tag{12}$$

where $\tau_p = \rho^s/\beta$ is the particle response time, $\tau_l = k^f/(6\epsilon^f)$ is the characteristic time scale of energetic eddies. Considering a given particle encounters an eddy on its path, if the particle is of very small inertia ($St \ll 1$), the particle can follow the eddy motion closely. If

Table 1: List of coefficients in fluid turbulence closure

C_μ	$C_{1\epsilon}$	$C_{2\epsilon}$	$C_{3\epsilon}$	$C_{4\epsilon}$	σ_k	σ_ϵ	σ_c
0.09	1.44	1.92	1.2	0 or 1.0	1.0	1.3	1.0

$St{\sim}O(1)$, the eddy can cause a significant disturbance on the particles trajectory. Finally, if $St \gg 1$, the particle can leave the swirling flow with its path hardly affected. *Danon et al.* (1977) and *Chen and Wood* (1985) proposed an exponential function for α:

$$\alpha = e^{-B \cdot St} \tag{13}$$

where B is an empirical coefficient. The last term in equation (10) represents the effect of sediment-induced density stratification on turbulence. It is typically a dissipation mechanism for the turbulent kinetic energy. According to the experimental evidence, it is also possible that the presence of particle provides a generation mechanism of flow turbulence. However, this is typically observed for very large Stokes number and this effect is neglected here.

The turbulent eddy viscosity is calculated as:

$$\nu^{ft} = C_\mu \frac{(k^f)^2}{\epsilon^f} \tag{14}$$

where C_μ is an empirical coefficient (see Table 1). The coefficients adopted here are listed in Table 1. As in *Hsu et al.* (2004), due to the lack of sufficient experimental data to provide appropriate empirical coefficients for particle-laden flow, the coefficients from the clear fluid $k - \epsilon$ model are used. For stable stratification $C_{4\epsilon} = 0$ is used following what typically used in stratified flow studies, however it is set to 1 for unstably stratified condition. Moreover, following *Hsu et al.* (2004) the coefficient $C_{3\epsilon}$ is chosen to be 1.2 and the coefficient B is left as the only free parameter in the model to be calibrated with measured data.

2.4 Closures on Particle Stresses

Following the conceptual plot shown in Figure 1, the closures of particle pressure and particle stresses include two components. For moderate sediment concentration, intergranular interaction is assumed to be caused by binary collisions and a closure based on kinetic theory is adopted. For large sediment concentration, binary collision eventually become invalid and intergranular interaction is dominated by enduring contact/frictional forces among particles. Hence, particle pressure and particle stress both consist of a collisional-

kinetic component and a frictional component (*Johnson and Jackson*, 1987; *Hsu et al.*, 2004):

$$p^s = p^{sc} + p^{sf} \tag{15}$$

$$\tau_{ij}^s = \tau_{ij}^{sc} + \tau_{ij}^{sf} \tag{16}$$

The collisional component based on the kinetic theory is first discussed. In the kinetic theory, particle stress and particle pressure are quantified by particle velocity fluctuations due to binary collisions. To quantify the strength of the particle velocity fluctuation, the concept of granular temperature Θ is introduced (*Jenkins and Savage*, 1983) for dry granular flow consists of smooth, slightly inelastic, spherical particles. In the present two-phase flow condition, we adopted the balance equation for granular temperature suggested by *Ding and Gidaspow* (1990):

$$\frac{3}{2}\Big[\frac{\partial \phi \rho^s \Theta}{\partial t} + \frac{\partial \phi \rho^s u_j^s \Theta}{\partial x_j}\Big] = \big(- p^{sc}\delta_{ij} + \tau_{ij}^{sc}\big)\frac{\partial u_i^s}{\partial x_j} - \frac{\partial q_j}{\partial x_j} - \gamma_s + J_{int} \tag{17}$$

where q_j is the flux of granular temperature, γ_s is the energy dissipation rate due to inelastic collision and J_{int} is the production (or dissipation) due to the interaction with the carrier fluid phase.

Since the kinetic theory is based on the assumption of binary collision, we need to introduce a function to describe the probability of the binary collision as a function of particle concentration. This is the radial distribution function g_{s0}. The basic requirement of the radial distribution function is that g_{s0} is a function of sediment concentration ϕ, and we need to ensure that g_{s0} goes to 1 when the ϕ approaches to 0, and g_{s0} goes to infinity when the ϕ approaches the packing limit. In this study, we use the radial distribution function for dense rigid spherical gases of *Carnahan and Starling* (1969):

$$g_{s0} = \frac{2 - \phi}{2(1 - \phi)^3} \tag{18}$$

It has been demonstrated that the formula of *Carnahan and Starling* (1969) under predicts g_{s0} when concentration $\phi > 0.57$ (*Ding and Gidaspow*, 1990; *Sinclair and Jackson*, 1989). However, it is noted here that in the present study when $\phi > 0.57$, the sediment stress are dominated by enduring contact/frictional component and the collisional component modeled by the kinetic theory reduces to zero at high concentration. Therefore, we still adopt the radial distribution function of *Carnahan and Starling* (1969) for simplicity.

In the 1980s, dense phase kinetic theory of gases (*Chapman and Cowling*, 1970) was applied to granular flow by many researchers (*Jenkins and Savage*, 1983; *Lun et al.*, 1984).

To apply the kinetic theory of granular flow to a wide range of particle concentration, *Lun et al.* (1984) demonstrated that particle pressure and particle stress due to collision consist of the kinetic part (similar to Reynolds stress) and a direct collisional part. In the present study, we adopt the closure of particle pressure proposed later by *Ding and Gidaspow* (1990):

$$p^{sc} = \rho^s \phi[1 + 2(1+e)\phi g_{s0}]\Theta \tag{19}$$

where e is the coefficient of restitution during the collision. Similarly, the corresponding particle stress is calculated by (*Gidaspow*, 1994):

$$\tau_{ij}^{sc} = \mu^{sc}\big[\frac{\partial u_i^s}{\partial x_j} + \frac{\partial u_j^s}{\partial x_i}\big] + \big(\lambda - \frac{2}{3}\mu^{sc}\big)\frac{\partial u_k^s}{\partial x_k}\delta_{ij} \tag{20}$$

The bulk viscosity is calculated as:

$$\lambda = \frac{4}{3}\phi^2 \rho^s d g_{s0}(1+e)\sqrt{\frac{\Theta}{\pi}} \tag{21}$$

The solid phase shear viscosity is calculated as the sum of kinetic shear viscosity and collisional shear viscosity:

$$\mu^{sc} = \rho^s d\sqrt{\Theta}\big[\frac{4}{5}\frac{\phi^2 g_{s0}(1+e)}{\sqrt{\pi}} + \frac{\sqrt{\pi} g_{s0}(1+e)\phi^2}{15} + \frac{\sqrt{\pi}\phi}{6} + \frac{5}{48}\frac{\sqrt{\pi}}{(1+e)g_{s0}}\big] \tag{22}$$

The closure of granular temperature flux is assumed to be analogous to the Fourier's law of conduction:

$$q_j = -\kappa\frac{\partial \Theta}{\partial x_j} \tag{23}$$

where the κ is the conductivity of granular temperature, calculated as

$$\kappa = \rho^s d\sqrt{\Theta}\big[\frac{2\phi^2 g_{s0}(1+e)}{\sqrt{\pi}} + \frac{9\sqrt{\pi} g_{s0}(1+e)\phi^2}{16} + \frac{15\sqrt{\pi}\phi}{16} + \frac{25}{64}\frac{\sqrt{\pi}}{(1+e)g_{s0}}\big] \tag{24}$$

Jenkins and Savage (1983) were the first study to model the dissipation rate due to inelastic collision. In this study, we use the closure later proposed by *Ding and Gidaspow* (1990):

$$\gamma_s = 3(1-e^2)\phi^2 \rho^s g_{s0}\Theta\big[\frac{4}{d}\big(\frac{\Theta}{\pi}\big)^{1/2} - \frac{\partial u_j^s}{\partial x_j}\big] \tag{25}$$

Due to the presence of carrier fluid phase, carrier flow turbulence can also induce particle fluctuations. According to *Ding and Gidaspow* (1990) and the turbulence closure discussed in the previous section, the fluid-particle interaction term can be expresses as:

$$J_{int} = \phi\beta(2\alpha k^f - 3\Theta) \tag{26}$$

When the volumetric concentration of particles becomes close to random loose packing ($\phi \approx 0.57$), particles are constantly in contact with each other, and particle energy can be dissipated by friction between sliding particles (*Tardos*, 1997). Thus, when the sediment concentration exceeds certain threshold value, frictional stress model need to be adopted. Following *Johnson and Jackson* (1987), the frictional component of particle pressure is calculated as:

$$p^{sf} = \begin{cases} 0, \phi < \phi_f \\ F\frac{(\phi-\phi_f)^m}{(\phi_{max}-\phi)^n}, \phi \geq \phi_f \end{cases} \tag{27}$$

where $\phi_f = 0.57$, $\phi_{max} = 0.635$ and F, m and n are empirical coefficients to be discussed later. The particle stress due to frictional effect is calculated by:

$$\tau_{ij}^{sf} = \mu^{sf}\left[\frac{\partial u_i^s}{\partial x_j} + \frac{\partial u_j^s}{\partial x_i}\right] - \frac{2}{3}\mu^{sf}\frac{\partial u_k^s}{\partial x_k}\delta_{ij} \tag{28}$$

where μ^{sf} is the frictional viscosity. *Srivastava and Sundaresan* (2003) combine the frictional normal stress model of *Johnson and Jackson* (1987) and the frictional viscosity model of from *Schaeffer* (1987). Thus, the friction viscosity is calculated by:

$$\mu^{sf} = \frac{\sqrt{2}p^{sf}\sin(\theta_f)}{2\sqrt{S_{ij}^s \cdot S_{ij}^s}} \tag{29}$$

where S_{ij}^s is the deviatoric part of strain rate tensor for sediment phase:

$$S_{ij}^s = \frac{1}{2}\left(\frac{\partial u_i^s}{\partial x_j} + \frac{\partial u_j^s}{\partial x_i}\right) - \frac{1}{3}\frac{\partial u_k^s}{\partial x_k}\delta_{ij} \tag{30}$$

In the above equation, θ_f is the angle of repose and is taken to be $\theta_f = 28^\circ$ for sand.

In sediment transport, the frictional component of particle pressure and particle stress play a definite role to ensure the existence of an immobile sediment bed and a low mobility layer of enduring contact can be modeled (*Hsu et al.*, 2004). Hence, the empirical coefficients presented here are calibrated to ensure that a stable sediment bed can be established below the mobile transport region. In the closure of particle pressure in the region of enduring contact, the following values are adopted in this study: $F = 0.05$, $m = 3$,

$n = 5$. Notice that in the original model of *Johnson and Jackson* (1987) applied to debris flow, these coefficients were suggested to be $F = 0.05$, $m = 2$ and $n = 5$. Therefore, the present model applied to sediment transport in a bottom boundary layer gives similar empirical values.

3 Numerical Method

The numerical implementation of the present formulations is based on an open-source CFD library called OpenFOAM, which provides a variety of finite volume method (FVM) libraries and solvers. OpenFOAM includes several single phase and multiphase flow modeling capabilities. Specifically, a two-phase flow solver in OpenFOAM called, twoPhaseEulerFoam (*Rusche*, 2002; *Weller*, 2002; *Peltola*, 2009) is adopted as the baseline. FVM uses the integral form of the conservation equations, dividing the domain into small control volumes (CV) and applying the conservation equation to each CVs. Volume and surface integrals are approximated with adequate quadrature formulas considering the center of the CV as the computational node and obtaining values at the CV faces through different interpolation schemes using the nodal values. This procedure results in the definition of one algebraic equation for each CV and leads to a conservative method by construction.

OpenFOAM uses the FVM over a collocated grid arrangement. The collocated arrangement stores all dependent variables at the cell center and the same CVs are used for all variables, so that the computational effort is minimized. A different approach is used in the staggered grid arrangement where different variables can be defined on different grids. Comparing to the staggered grid system, the main advantages of collocated arrangement are a minimization of the computational effort since all variables are stored using the same CV and an effective treatment of complex domains, especially with discontinuous boundary conditions. In addition, the difficulties linked to the pressure-velocity coupling and the consequent oscillations in the pressure fields are resolved through the Rhie and Chow method (*Rhie and Chow*, 1983).

3.1 Finite Volume Discretization

The momentum equations in the conservative form (equation (3) and (4)) are expanded into the non-conservative form for numerical convenience. For example, in fluid momentum equation (3), expanding the left-hand-side (LHS) of equation and substituting equation (1) into equation (3) yields the momentum equations in the non-conservative form:

$$\frac{\partial u_i^f}{\partial t} + u_j^f \frac{\partial u_i^f}{\partial x_j} = -\frac{1}{\rho^f}\frac{\partial p^f}{\partial x_i} + \frac{1}{\rho^f(1-\phi)}\frac{\partial (1-\phi)\tau_{ij}^f}{\partial x_j} - \frac{\phi\beta u_i^f}{\rho^f(1-\phi)} + F_i^f \qquad (31)$$

where $F_i^f = g\delta_{i3} + \frac{\phi\beta u_i^s}{\rho^f(1-\phi)} + \frac{\beta}{\rho^f(1-\phi)}\frac{\nu^{ft}}{\sigma_c}\frac{\partial \phi}{\partial x_i}$ is a sum of gravitational term, drag term and turbulent suspension term. The non-conservative form of the sediment momentum equation can be derived in a similar way:

$$\frac{\partial u_i^s}{\partial t} + u_j^s \frac{\partial u_i^s}{\partial x_j} = -\frac{1}{\rho^s}\frac{\partial p^f}{\partial x_i} + \frac{1}{\rho^s \phi}\frac{\partial \tau_{ij}^s}{\partial x_j} - \frac{\beta u_i^s}{\rho^s} + F_i^s \tag{32}$$

where $F_i^s = -\frac{1}{\rho^s \phi}\frac{\partial p^s}{\partial x_i} + g\delta_{i3} + \frac{\beta u_i^f}{\rho^s} - \frac{\beta}{\rho^s \phi}\frac{\nu^{ft}}{\sigma_c}\frac{\partial \phi}{\partial x_i}$ is a sum of particle pressure gradient, gravitational term, drag term and turbulent suspension term. To illustrate the finite volume discretization, we can take equation (31) as an example. Expanding the second term on the RHS of equation (31), and substituting equation (9) yields:

$$\begin{aligned}\frac{1}{\rho^f(1-\phi)}\frac{\partial(1-\phi)\tau_{ij}^f}{\partial x_j} = \frac{\nu^{eff}}{(1-\phi)}\frac{\partial(1-\phi)}{\partial x_j}\frac{\partial u_i^f}{\partial x_j} + \frac{\nu^{eff}}{(1-\phi)}\frac{\partial(1-\phi)}{\partial x_j}T_{ij} \\ + \frac{\partial}{\partial x_j}\left(\nu^{eff}\frac{\partial u_i^f}{\partial x_j}\right) + \frac{\partial T_{ij}}{\partial x_j}\end{aligned} \tag{33}$$

where $T_{ij} = \nu^{eff}\frac{\partial u_j^f}{\partial x_i} - \frac{2}{3}\left(k^f + \frac{\partial u_k^f}{\partial x_k}\right)\delta_{ij}$. Through the above expansion, the first term on the RHS of equation (33) can be combined with the convection term on the LHS of equation (31). This diffusive term can avoid high fluctuations near sharp concentration gradient, and make the solver more stable. As we will provide more details later, the standard PISO procedure is used in the present solver. The intermediate velocities are solved from the momentum equation without the pressure gradient term, and then the velocities are corrected after the pressure is solved to satisfy mass conservation. Firstly, equation (31) without pressure gradient term can be further rearranged, and volume integral of the divergence terms are transferred to surface integral over the control surface (CS) through Gauss's theorem. Thus, the following semi-discretized system of equations can be derived:

$$\begin{aligned}\int_{CV}\frac{\partial u_i^{f*}}{\partial t}dV + \oint_{CS} u_j^T n_j u_i^{f*} dS - u_i^{f*}\oint_{CS} u_j^T n_j dS = \oint_{CS}\nu^{eff}\frac{\partial u_i^{f*}}{\partial x_j}dS \\ + \oint_{CS} T_{ij} n_j dS + \int_{CV} H_i dV\end{aligned} \tag{34}$$

where n_j is the jth component of the unit vector orthogonal to CS and directed outwards, $u_j^T = u_j^f - \frac{\nu^{eff}}{(1-\phi)}\frac{\partial(1-\phi)}{\partial x_j}$, and $H_i = F_i^f - \frac{\phi\beta u_i^{f*}}{\rho^f(1-\phi)} + \frac{\nu^{eff}}{(1-\phi)}\frac{\partial(1-\phi)}{\partial x_j}T_{ij}$ are source terms in the momentum equations. The $*$ symbol represents intermediate quantities in the projection scheme. A similar rearrangement can also be applied to the momentum equation for sediment phase (equation (4)). The discretization for the other governing equations such as equation (2, 10, 11, 17) are similar, and they are not repeated here.

3.2 Projection Method

As mentioned before, the standard projection method is used to solve fluid and particle velocities (*Rusche*, 2002; *Weller*, 2002; *Peltola*, 2009). Firstly, the intermediate velocities (u_i^{f*},u_i^{s*}) are calculated by the corresponding momentum equations without pressure gradient terms:

$$u_i^{f*} = \frac{A_{Hi}^f}{A_D^f} + \frac{F_i^f}{A_D^f} \tag{35}$$

$$u_i^{s*} = \frac{A_{Hi}^s}{A_D^s} + \frac{F_i^s}{A_D^s} \tag{36}$$

where F_i^f and F_i^s are source terms defined in equation (31) and (32), A_D^f and A_{Hi}^f are coefficient matrices arising from the discretization of fluid momentum equation (equation (31)) without fluid pressure gradient term and F_i^f term. A_D^s and A_{Hi}^s are similar coefficient matrices associated with sediment momentum equation (equation (32)) excluding fluid pressure gradient term and F_i^s term. The reason for separating fluid pressure term and source term (F_i^f and F_i^s) from the momentum equations is explained as follow: the momentum equations are constructed using cell center variables, and it has been noticed that treating gradient terms such as turbulent suspension and gradient of particle normal stress and explicit drag terms at cell faces are beneficial for numerical stability. Thus, these terms are not included in the construction of coefficient matrices A_D^f, A_{Hi}^f, A_D^s and A_{Hi}^s.

These intermediate velocities do not satisfy the mass conservation equations (equations (1), (2)). To enforce mass conservation of each phase, the pressure equation is constructed by considering the continuity equations for both phases. In the present model, method of *Rhie and Chow* (1983) has been adopted for pressure equations to prevent velocity-pressure decoupling and oscillation in pressure fields. The pressure equations are constructed using velocity flux field, thus the continuity equation is formulated at the cell faces as

$$\frac{\partial\big[(1-\phi_f)\Phi^f + \phi_f\Phi^s\big]}{\partial x_i} = 0 \tag{37}$$

where the subscript f denotes variables interpolated to the cell faces, Φ^f and Φ^s are fluid and sediment velocity fluxes at cell faces, respectively. Finally, the following pressure equation can be obtained:

$$\frac{\partial}{\partial x_i}\Big[\Big(\frac{\phi_f}{\rho^s(A_D^s)_f} + \frac{1-\phi_f}{\rho^f(A_D^f)_f}\Big)\frac{\partial p^f}{\partial x_i}\Big] = \frac{\partial\big[(1-\phi_f)\Phi^{f*} + \phi_f\Phi^{s*}\big]}{\partial x_i} \tag{38}$$

where Φ^{f*} and Φ^{s*} are flux prediction by interpolating intermediate fluid velocity and sediment velocity to the faces. After solving the pressure, the fluid and sediment velocities are updated as

$$u_i^f = u_i^{f*} - \frac{1}{\rho^f A_D^f} \frac{\partial p^f}{\partial x_i} \tag{39}$$

$$u_i^s = u_i^{s*} - \frac{1}{\rho^s A_D^s} \frac{\partial p^f}{\partial x_i} \tag{40}$$

The resulting fluid phase and particle phase velocities now satisfy mass conservation.

3.3 Sediment Concentration Equation

Following the rearrangement of *Weller* (2002), the conservative form of sediment continuity equation (2) can be written as

$$\frac{\partial \phi}{\partial t} + \frac{\partial \phi U_i}{\partial x_i} + \frac{\partial \phi(1-\phi) U_{ri}}{\partial x_i} = 0 \tag{41}$$

where $U_i = (1-\phi)u_i^f + \phi u_i^s$, and $U_{ri} = u_i^f - u_i^s$. In the second term, ϕ is bounded since the mixture velocity U satisfy the mixture continuity equation exactly. In the third term, the two phases are coupled implicitly through the presence of the relative velocity U_r, and bounding of ϕ is achieved by using U_r in the convection scheme to interpolate ϕ to the face (and use $-U_r$ to interpolate $(1-\phi)$ to the face). This treatment is quite diffusive if first order differencing scheme is used. Hence, higher order differencing scheme should be used.

3.4 Time Step Control

At the beginning of each cycle, the time step is adjusted such that it is sufficiently small to ensure the stability of the numerical solution procedure. In the present two-phase flow framework, the time step is usually constrained by the Courant number Co at a cell face:

$$Co = max\left\{ \left| \frac{u_i^s \Delta t}{\Delta L_i} \right|, \left| \frac{u_i^f \Delta t}{\Delta L_i} \right| \right\} \tag{42}$$

where ΔL_i is the ith component of vector between two neighboring cell centers. Since the relative velocity is also important in the concentration equation, a Courant number based on the relative velocity is also defined:

$$Co_r = \left| \frac{(u_i^s - u_i^f)\Delta t}{\Delta L_i} \right| \tag{43}$$

The time step should be adjusted in a smooth fashion to ensure the numerical stability as well as better convergence. Under-relaxation is proven to beneficial to achieve this goal. Meanwhile, a maximum time step is also defined to avoid very large time step. This control prescription is defined to be:

$$\Delta t^n = \begin{cases} \Delta t^t, Co > Co^t \; or \; Co_r > Co_r^t \\ min\Big\{min\Big[min\Big(\Delta t^t, \Delta t^o + 0.1\Delta t^t\Big), 1.2\Delta t^o\Big], \Delta t^m\Big\}, otherwise \end{cases} \tag{44}$$

where Co^t and Co_r^t are the target Courant number for Co and Co_r, respectively. Δt^o and Δt^n are time step of previous time step and new time step, respectively, $\Delta t^t = min\Big\{\frac{Co^t}{Co^o}, \frac{Co_r^t}{Co_r^o}\Big\}\Delta t^o$, and Δt^m is the maximum allowed time step.

3.5 Program Outline and Flow Chart

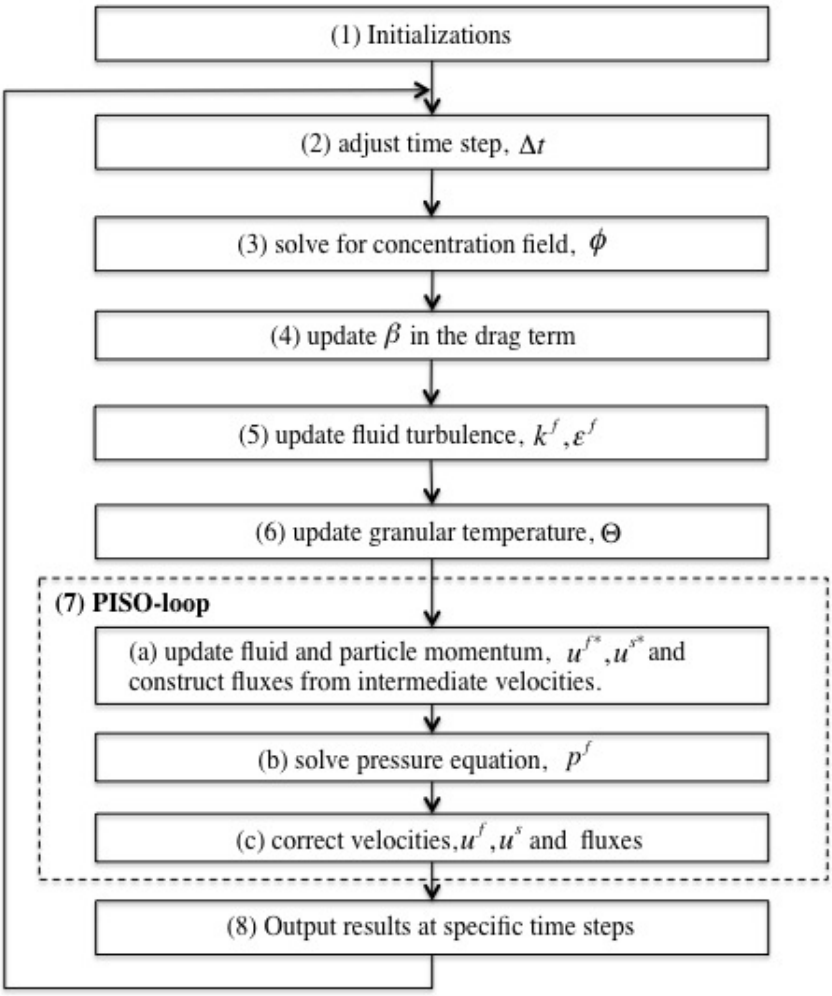

Figure 2: Flow chart of solution procedure

The solution procedure is outlined in the Figure 2, and the sequence of solution is summarized as follow:

(1) Initializations: initialize all the variables;

(2) Adjust the time step according to Courant number, $Co < 0.3$ and $Co_r < 0.1$;

(3) Solve for sediment concentration, i.e., equation (41);

(4) Calculate β in the drag term, i.e., equation (7);

(5) Solving $k - \epsilon$ equations in turbulence closure, i.e., equations (10, 11);

(6) Solving granular temperature, i.e., equation (17);
(7) PISO-loop, solving velocity-pressure coupling:
  (a) Calculate u_i^{f*},u_i^{s*} using equations (35, 36) without fluid pressure gradient term;
  (b) Construct and solve the pressure equation (38);
  (c) Correct fluid and particle velocities after solving pressure, i.e., equation (39, 40) and update fluxes;
(8) Output results at defined output sequences.

3.6 A Summary of Major Modifications

As mentioned before, the present numerical model is modified from the solver twoPhaseEulerFoam (*Rusche*, 2002; *Weller*, 2002; *Peltola*, 2009). New terms are added so that the model solves the model formulation presented in Section 2. The solution procedure is also revised to make the solver more robust. For example, the fluid turbulence is updated immediately after solving the sediment concentration field, and then the kinetic theory of granular flow is solved. In this manner, the fluid and particle turbulence are better coupled. Meanwhile, the concentration field is updated only once, and shared by all the subsequent procedures.

The gradient terms such as turbulent suspension term and particle normal stress term are treated at the cell faces. In this manner, the discretization of the gradients are performed for each face, and it's numerically more stable. Meanwhile, the drag terms due to mean motions are treated implicitly. In the PISO loop, the explicit parts of drag terms are updated after each inner loop, so that the Newton third law are satisfied and inter-phase coupling are better resolved. Meanwhile, the production terms in $k-\epsilon$ equations (equations (10) and (11)) and granular temperature equations (equation (17)) are treated implicitly to ensure numerical stability.

A frictional stress model named **SrivastavaSundaresan** is adopted for sediment transport application. This model combines the frictional normal stress from *Johnson and Jackson* (1987) and tangential stress model from *Schaeffer* (1987). This new model has the capability to capture the transition of solid-like feature to fluid-like feature of the sediment bed. This frictional stress is implemented explicitly in the sediment momentum equation (4). Moreover, with this new frictional stress model, the sediment concentration rarely exceeds the maximum packing limit (usually around 0.635).

Meanwhile, following Rhie-chow's procedure of pressure correction with collocated grids, the pressure field is solved using intermediate velocity flux field. After solving for pressure field, pressure gradient are calculated at cell faces and then the velocity is corrected. This procedure is taken here instead of directly reconstructing the flux field, which is known to be highly dissipative.

4 Model Examples/Validations

The model is first calibrated/validated with laboratory flume data of *Sumer et al.* (1996) for sand transport in steady channel flow under sheet flow condition. Then, the calibrated model is demonstrated to reproduce measured sheet flow data of *O'Donoghue and Wright* (2004) for oscillatory flow.

4.1 Steady Sheet Flow

Comparing to *Hsu et al.* (2004), the present model adopted a new turbulence modulation model in $k-\epsilon$ equations as well as in the granular temperature equation. This model is expected to be more robust in predicting the sediment suspension for a wider range of sediment grain size. The numerical model is validated with sheet flow data driven by steady channel flow measured by *Sumer et al.* (1996) for two types of sediment. Specifically, the model coefficient B (see equation (13)) associated with turbulence modulation due to sediment is calibrated using this dataset.

Conventionally, the non-dimensional bed shear stress, called the Shields parameter, is used to quantify non-cohesive sediment transport. For steady channel flow, the Shields parameter can be calculated using bottom stress (or friction velocity), sediment density and diameter:

$$\theta = \frac{\tau_b}{(\rho^s - \rho^f)gd} = \frac{u_*^2}{(s-1)gd} \tag{45}$$

In the numerical simulation, the driven force is the streamwise pressure gradient, which can be determined by the energy slope ξ in an open channel flow experiment:

$$\frac{1}{\rho^f}\frac{\partial \bar{p}^f}{\partial x} = -g\xi \tag{46}$$

In *Sumer et al.* (1996), the bed friction velocity u_* is calculated using the energy slope ξ and hydraulic radius r_b associated with the flume:

$$u_*^2 = -g\xi r_b \tag{47}$$

The results of fine sand transport from *Sumer et al.* (1996) are presented here. When using $B = 0.15$, we obtain good agreement with measured sediment concentration profile for a range of Shields parameter fine sand. Figure 3 shows the model result from the 1DV model setup (only 1 grid points in streamwise and spanwise direction). For three cases of fine sand (d=0.13 mm, s=2.65), it can be observed from panel (a1), (a2) and (a3) in Figure 3 that the particle shear stress increases rapidly in the sheet layer until

reaching the bed while the fluid shear stress drops sharply in the sheet flow layer and becomes close to zero at the bed. The summation of particle shear stress and fluid (mostly turbulent) shear stress gives the expected linear profile of total shear stress in a steady channel flow. The comparisons of concentration profile are shown in panel (b1), (b2) and (b3) in Figure 3. With the calibrated $B = 0.15$, the agreement between the model results (curves) and measured data (symbols) is reasonably well for Shields parameter in the range of $1.1 \sim 2.2$. Panel (c1), (c2) and (c3) shows the velocity profile of fluid (curves) and sediment phase (circles), due to the lack of experimental data for velocity profile, the validation is merely based on the concentration profiles.

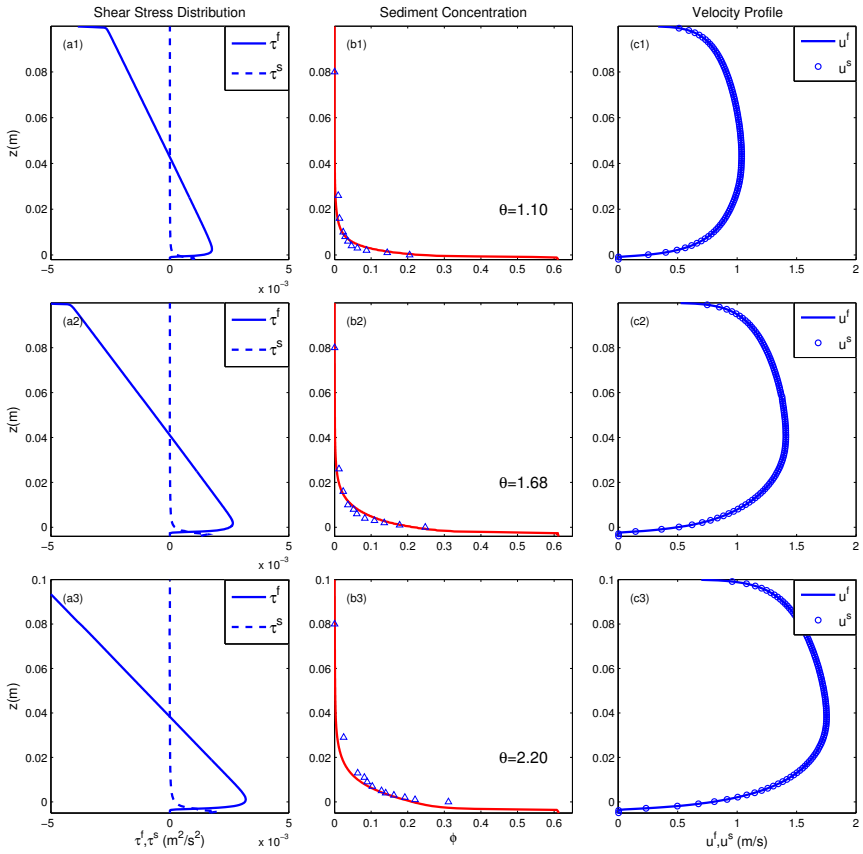

Figure 3: Model-data comparison for steady sheet flow of Sumer et al. (1996). Panels (a1), (b1), (c1) ((a2), (b2), (c2) or (a3), (b3), (c3)) are results for $\theta = 1.1$ ($\theta = 1.68$ or 2.2)

Table 2: Flow conditions in *O'Donoghue and Wright* (2004)

Flow condition	T(s)	A(m)	a	U_m(m/s)
Sinusoidal	5	1.2	0.5	1.5
Asymmetric	7.5	1.5	0.63	1.5

4.2 Oscillatory Sheet Flow

O'Donoghue and Wright (2004) measured sediment concentration in both the bedload and suspended load regions under oscillatory sheet flow for a range of flow condition and three different grain sizes. This dataset has been used by many other researchers to validate their models (*Li et al.*, 2008; *Chen et al.*, 2011; *Yu et al.*, 2012) and it is used to validate the present model. Medium sand ($d = 0.28$mm) under symmetric and asymmetric flow conditions are modeled (see Table 2).

The oscillatory flow is driven by a mean streamwise pressure gradient. Outside the wave boundary layer, the shear stress vanishes, and the momentum equation reduces to:

$$\frac{1}{\rho^f}\frac{\partial \bar{p}^f}{\partial x} = -\frac{\partial U_0}{\partial t} \tag{48}$$

where U_0 is the free stream velocity. For sinusoidal wave, $U_0 = U_m \sin(\omega t)$, and U_m is the free-stream velocity magnitude. For asymmetric flow, the flow is forced by the second-order Stokes wave motion:

$$U_0 = U_1 \sin(\omega t) - U_2 \cos(2\omega t) \tag{49}$$

where U_1, U_2 are velocity amplitudes for 1st and 2nd harmonics, $\omega = 2\pi/T$ is the wave frequency, and T is the wave period. The flow asymmetry is defined as: $a = U_{max}/(U_{max} - U_{min})$, in which U_{max} and U_{min} are maximum and minimum free-stream velocities, respectively, and semi-excursion length A is calculated as $A = U_0/\omega$.

Medium Sand, sinuoidal wave, $T = 5$ **s**: In Figure 4, the concentration profiles at maximum onshore (c) and offshore (e) velocities and flow reversals ((b) and (d)) are compared with the experimental data of *O'Donoghue and Wright* (2004). Both 1DV (blue solid curves) and 2DV (red dashed curves) results are shown. We can see that 1DV and 2DV results are almost identical and they both agree quite well with the measured data. We like to note that this agreement is achieved with $B = 0.15$ without further tuning. It is found that for medium sand grain, more sand is suspended during the flow peak (flow is strong) than the flow reversal (flow is weak).

In Figure 5, the time series of concentration at three different vertical locations are shown. Time series of concentration from dense region (panel a), close to initial bed level

(panel b), and away from the initial bed level (panel c) are compared with measured data from *O'Donoghue and Wright* (2004). The model is shown to predict the evolution of concentration well at these representative locations. It is observed that sediment in the dense region (see panel a) is eroded and suspended when the flow is intense (around flow peak) and as a result, suspended sediment in dilute region (see panel c) becomes larger around the flow peak. When the flow becomes weak, suspended sediment settles to the bed, thus sediment concentration in dilute region reduces while bed level increase (see panel a). 1DV (blue solid curves) and 2DV (red dashed curves) results are again very similar.

Figure 6 shows 2DV model results for the contour of the concentration field during (a) flow reversal and (b) flow peak. The arrows represent the velocity vectors, and the length of the arrows scale with its magnitude. We can see that the concentration and velocity are homogeneous in the streamwise direction, consistent with typical expectation of turbulence-averaged sheet flow. This also explains the reason that 1DV and 2DV model results are identical. It is commented here that the 2DV turbulence-averaged model results can reproduce the expected homogeneous sheet flow in the streamwise direction suggesting that the numerical solver is quite stable.

Medium Sand, 2nd-order Stokes wave, $T = 7.5$ **s**: Skewed free-stream velocity is one of the main mechanisms driven onshore sediment transport. Concentration profiles at the four representative phases are shown in Figure 7. The overall agreement between measured data and model results are very good. Time series of concentration (Figure 8) at three different locations are also compared well with measured data. Again, both 1DV model results and 2DV model results are shown and they are basically identical.

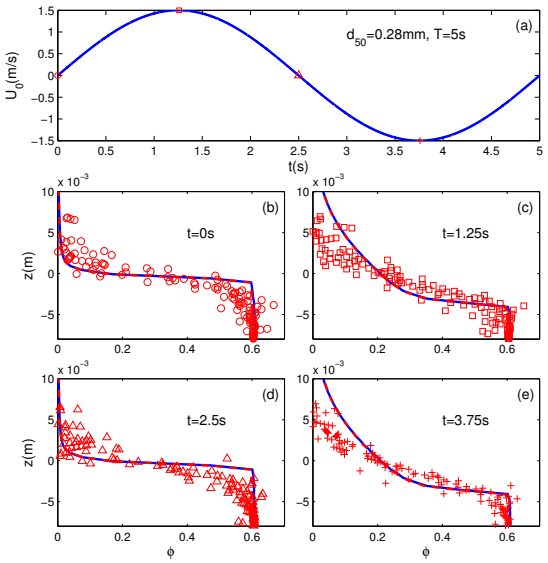

Figure 4: Comparison of predicted (curves) and measured (symbol) concentration profiles at four different instants for sheet flow of medium sand driven by sinusoidal motion (T=5.0 sec and U_m=1.5 m/s, *O'Donoghue and Wright* (2004))

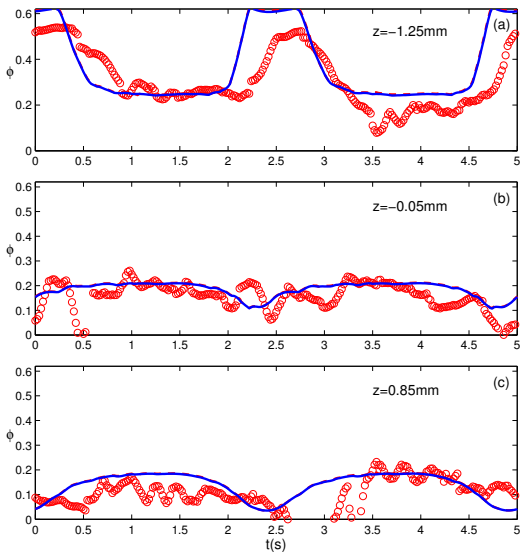

Figure 5: Comparison of concentration time series at three different vertical locations for sheet flow of medium sand driven by sinusoidal motion (T=5.0 sec and U_m=1.5 m/s, *O'Donoghue and Wright* (2004))

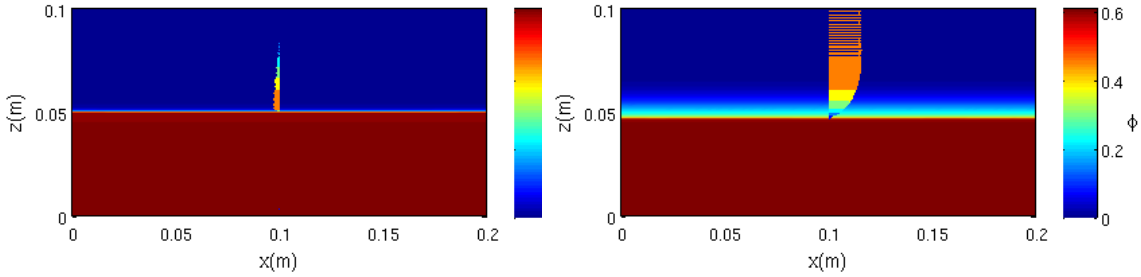

(a) Flow reversal (t=0 s)

(b) Flow peak (t=1.25 s)

Figure 6: Snapshot of concentration field at (a) flow reversal (t=0 s) and (b) flow peak (t=1.25 s) for sheet flow of medium sand driven by sinusoidal motion

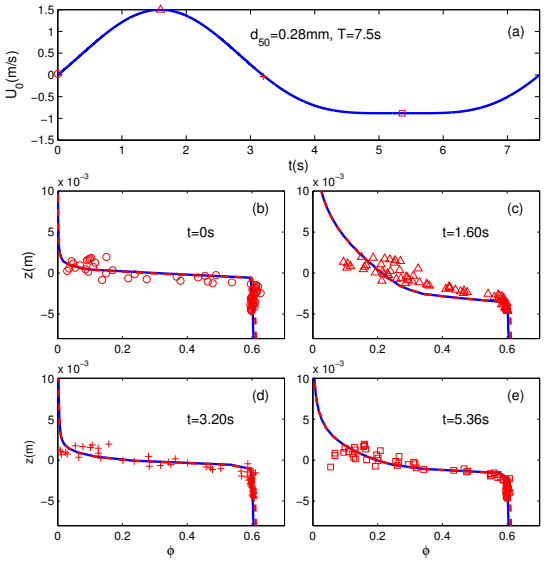

Figure 7: Comparison of predicted (curves) and measured (symbols) concentration profiles at four different instants for sheet flow of medium sand driven by Stokes 2nd-order wave motion (T=7.5 sec, *O'Donoghue and Wright* (2004))

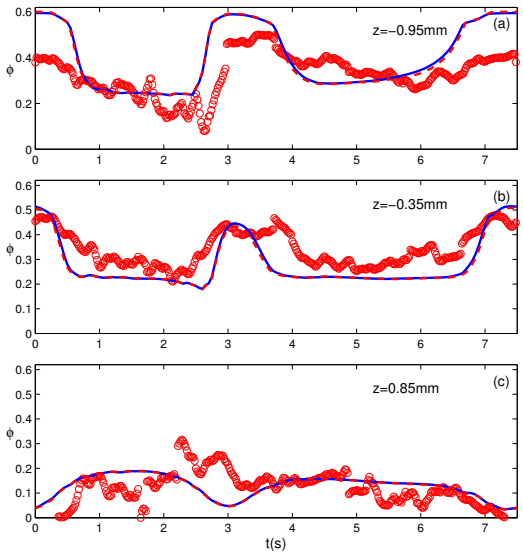

Figure 8: Comparison of concentration time series at three different vertical locations for sheet flow of medium sand driven by Stokes 2nd-order wave motion (T=7.5 sec, *O'Donoghue and Wright* (2004))

5 Conclusion and Future Work

A multi-dimensional two-phase Eulerian model for sediment transport has been developed based on the open-source CFD library, OpenFOAM. The mathematical formulation follows the standard two-phase flow approach for sediment transport, and several modifications to the numerical solver are introduced to make the model more robust. This model can be applied to study sediment transport under steady channel flow, sinusoidal wave, 2nd-order Stokes waves, and wave plus current. Finally, this model is validated by comparing the experimental data of steady channel flow and wave tunnels (sinusoidal wave and 2nd-order Stokes wave), and good agreements have been achieved in terms of the prediction of sediment concentration.

However, there are several limitations of this model and future work is required. For example, this model is based on the $k - \epsilon$ turbulence closure and model results are quite sensitive to the closure coefficients. Future release will include 3D turbulence-resolving sediment transport using the Large-eddy simulation approach. By introducing twoPhaseEulerSedFoam as an open-source code, it is also our hope that more sediment transport researchers will be involved in the future development of the model for more complete (or alternative) model formulations and closures as well as wider sediment transport applications.

6 Appendix

6.1 Installation and Compilation

This solver is modified based on the twoPhaseEulerFoam solver in OpenFOAM-2.1.0, so make sure that OpenFOAM-2.1.0 has already been successfully installed, this version of OpenFOAM can be found through the following link:

http://www.openfoam.org/archive/2.1.0/download/

After installing OpenFOAM-2.1.0, the new solver twoPhaseEulerSedFoam can be compiled through the following procedure:

(1) twoPhaseEulerSedFoam is distributed in a compressed file. To install and compile the solver, first uncompress the package, the exacted files will be distributed in two new directories: /twoPhaseEulerSedFoam and /Example, and three files: license, README and User Manual.

(2) After uncompressing the .zip file, and copy the folder 'twoPhaseEulerSedFoam' to the directory: $FOAM_APP/solver/multiphase/.

(3) Enter the directory of twoPhaseEulerSedFoam, and type the following command to compile the solver:

./Allwmake

If OpenFOAM-2.1.0 has been successfully compiled, the new solver will start to compile, and the compilation may take several minutes to complete.

(4) After the compilation, a new solver is generated by the name of twoPhaseEulerSedFoam.

6.2 Model Input and Output

The example cases can be found in the /example within the uncompressed folder. In the example cases, one Steady channel flow case and two oscillatory flow cases can be found. That is, the current solver can be used to simulate sediment transport under steady flow or simple wave (sinusoidal and 2nd-order stokes wave). These flow conditions are driven by pressure gradient force, which is defined in **/constant/transportProperties**:

// * * * * * * * * * * * following are for driving force * * * * * * * * * * * //

tilt tilt [0 0 0 0 0 0 0] 1; //tiled tube or not?

gradPAMP1 gradPAMP1 [1 -2 -2 0 0 0 0] (0 0 0); // pressure osci amp1

gradPAMP2 gradPAMP2 [1 -2 -2 0 0 0 0] (0 0 0); // pressure osci amp2

gradPOSC gradPOSC [1 -2 -2 0 0 0 0] (46.9899 0 0); // pressure osci real value

gradPMEAN gradPMEAN [1 -2 -2 0 0 0 0] (46.9899 0 0); //mean pressure

```
    oscpT    oscpT   [ 0 0 0 0 0 0 0 ]   20; // osci period
    initTheta    initTheta   [ 0 0 0 0 0 0 0]   0; //initial deg

// * * * * * * definition of turbulence coefficient and others * * * * * //
    SUS    SUS   [ 0 0 0 0 0 0 0 ]   1; //set to 1 to include turbulent suspension term, else
set to 0
    C3ep    C3ep   [ 0 0 0 0 0 0 0 ]   1.2; //set the coefficient of C3 in epsilon equation */
    C4ep    C4ep   [ 0 0 0 0 0 0 0 ]   0;
    KE1    KE1   [ 0 0 0 0 0 0 0 ]   0; //density stra (Uf-Us), horizontal component
    KE2    KE2   [ 0 0 0 0 0 0 0 ]   1; //set to 1 to include turbulence modulation
    KE3    KE3   [ 0 0 0 0 0 0 0 ]   0; //turbulence generation, not included
    KE4    KE4   [ 0 0 0 0 0 0 0 ]   1; //density stratification g
    B    B   [ 0 0 0 0 0 0 0 ]   0.15; //turbulence modulation coefficient
    alphaMinFriction  alphaMinFriction   [ 0 0 0 0 0 0 0 ]   0.57;
// * * * * * * * * * * * * * end of definition * * * * * * * * * * * * * //

// * * * * * * * * * fluid and sediment properties * * * * * * * * * //
phasea
{
    rho    rho    [ 1 -3 0 0 0 ]    2650; // sediment density
    nu    nu    [ 0 2 -1 0 0 ]    2; // sediment viscosity, dummy
    d    d   [ 0 1 0 0 0 0 0 ]    0.00013; // sediment grain size (m)
}

phaseb
{
    rho    rho    [ 1 -3 0 0 0 ]    1000; // fluid density
    nu    nu   [ 0 2 -1 0 0 ]    1.e-06; //fluid viscosity
    d    d    [ 0 1 0 0 0 0 0 ]    0.00013; // fluid diameter, dummy
}
    Cvm    Cvm   [ 0 0 0 0 0 ]    0; // virtual mass coefficient
    Cl    Cl    [ 0 0 0 0 0 ]    0; // lift coefficient
    Ct    Ct    [ 0 0 0 0 0 ]    0; // turbulence response coefficient, not considered
    alphaAlpha    alphaAlpha   [ 0 0 0 0 0 ]   0; // contact angle, not considered
 // * * * * * * * * * * * * * end of definition in transportProperties* * * * * * * * * * * * * //
```

The coefficient and parameters in kinetic theory for granular flow are defined in **/constant/kineticTheoryProperties**:

kineticTheory on; // turn on kinetic theory for granular flow

equilibrium off; // turn off the equilibrium simplification of granular temperature equation

e e [0 0 0 0 0 0 0] 0.8; // coefficient of restitution

alphaMax alphaMax [0 0 0 0 0 0 0] 0.635; // maximum sediment concentration allowed

alphaMinFriction alphaMinFriction [0 0 0 0 0 0 0] 0.57; // threshold of enduring contact region

DiluteCut DiluteCut [0 0 0 0 0 0 0] 1e-8; // kinetic theory is not calculated when sediment concentration is below this value

ttzero ttzero [0 0 1 0 0 0 0] 0; // time start to relax kinetic theory to avoid initial instability

ttone ttone [0 0 1 0 0 0 0] 0; // end time for the relaxation

MaxTheta MaxTheta [0 2 -2 0 0 0 0] 0.05; // max granular temperature allowed

Fr Fr [1 -1 -2 0 0 0 0] 0.05; // coefficient F in Johnson-Jackson model, equation (27)

eta eta [0 0 0 0 0 0 0] 3; // coefficient m in Johnson-Jackson model, equation (27)

p p [0 0 0 0 0 0 0] 5; // coefficient n in Johnson-Jackson model, equation (27)

phi phi [0 0 0 0 0 0 0] 28.0; // internal friction angle of sediment

KineticJ1 KineticJ1 [0 0 0 0 0 0 0] 1; // set to 1 to turn on the model 1 for J_{int} in equation (17)

KineticJ2 KineticJ2 [0 0 0 0 0 0 0] 0; // set to 1 to turn on the model 2 for J_{int} in equation (17)

KineticJ3 KineticJ3 [0 0 0 0 0 0 0] 0; // set to 1 to turn on the model 3 for J_{int} in equation (17)

viscosityModel Gidaspow; // use Gidaspow's model for particle viscosity

conductivityModel Gidaspow; // use Gidaspow's model for particle conductivity

granularPressureModel Lun; // use Lun's model for granular normal stress (collisional part)

frictionalStressModel SrivastavaSundaresan; // use newly added frictional stress model (frictional part)

radialModel CarnahanStarling; // use Carnahan Starling's radial distribution model

HrenyaSinclairCoeffs // coefficient used in Hrenya and Sinclair's model

{

```
    L   L   [ 0 1 0 0 0 0 0 ]   0.0005;
}
```

The other files in **/constant/** are defined similar to twoPhaseEulerFoam, and the discussion is not repeated here, and the numerical schemes is defined in **/system/fvScheme**:

```
ddtSchemes
{
    default      CrankNicholson      0.5; // use Standard Crank Nicholson scheme for temporal integration
}

gradSchemes
{
    default      Gauss linear; // defaultly use central difference scheme
}

divSchemes
{
    default      none;
    div(phia,Ua)      Gauss limitedLinearV 1; // use TVD schemes for the convection terms
    div(phib,Ub)      Gauss limitedLinearV 1;
    div(phiRa,Ua)      Gauss limitedLinearV 1;
    div(phiRb,Ub)      Gauss limitedLinearV 1;
    div(phib,k)      Gauss limitedLinear 1;
    div(phib,epsilon)      Gauss limitedLinear 1;
    div(phib,beta)      Gauss limitedLinear01 1;
    div(phi,alpha)      Gauss limitedLinear01 1;
    div(phi,Theta)      Gauss limitedLinear 1;
    div(Rca)      Gauss linear;
    div(Rcb)      Gauss linear;
    div(phir,alpha)      Gauss limitedLinear01 1;
}
laplacianSchemes
{
    default      none;
    laplacian(nuEffa,Ua)      Gauss linear corrected;
    laplacian(nuEffb,Ub)      Gauss linear corrected;
    laplacian((rho*(1—A(U))),p)      Gauss linear corrected;
    laplacian(alphaPpMag,alpha)      Gauss linear corrected;
```

```
    laplacian(Galphaf,alpha)      Gauss linear corrected;
    laplacian(DkEff,k)      Gauss linear corrected;
    laplacian(DkEff,beta)      Gauss linear corrected;
    laplacian(DepsilonEff,epsilon)      Gauss linear corrected;
    laplacian(DepsilonEff,beta)      Gauss linear corrected;
    laplacian(kappa,Theta)      Gauss linear corrected;
}

interpolationSchemes
{
    default      linear;
}

snGradSchemes
{
    default      corrected;
}

fluxRequired
{
    default      no;
    p ;
}
```

Only the important features are discussed here, and other coefficients such as /system/fvSolution can be defines following the tutorial of OpenFOAM (*http://www.openfoam.org/docs/user/tutorials.php*)

The output sequence control can be defined in **/system/controlDict**, and the results are distributed in one folder named by output time or time step for each output. In each output, the following files can be found:

alpha: sediment concentration field
epsilon: fluid turbulence dissipation rate
k: fluid turbulent kinetic energy
nutb: turbulent viscosity
Theta: sediment granular temperature
p: fluid pressure field
Ua: sediment velocity field
Ub: fluid velocity field

U: mixture velocity field, $\phi u^s + (1-\phi)u^f$
Ur: relative velocity field, $u^f - u^s$
phia: sediment velocity flux field
phib: fluid velocity flux field
mua: sediment viscosity field
pa: sediment normal pressure field (collisional part))
gradPs: sediment pressure gradient (collisional part)
gradPf: sediment frictional pressure gradient (frictional part)
Tauf: total fluid shear stress field
Taus: particle shear stress field (collisional part)
tmf: turbulence modulation parameter
susb: turbulent suspension term in fluid momentum equation
/uniform: folder to log time step and runTime

References

Amoudry, L., and P.-F. Liu (2009), Two-dimensional, two-phase granular sediment transport model with applications to scouring downstream of an apron, *Coastal Engineering*, *56*(7), 693–702.

Amoudry, L. O., and P. L.-F. Liu (2010), Parameterization of near-bed processes under collinear wave and current flows from a two-phase sheet flow model, *Continental Shelf Research*, *30*(13), 1403–1416.

Bakhtyar, R., D. A. Barry, A. Yeganeh-Bakhtiary, L. Li, J.-Y. Parlange, and G. Sander (2010), Numerical simulation of two-phase flow for sediment transport in the inner-surf and swash zones, *Advances in water resources*, *33*(3), 277–290.

Balachandar, S., and J. K. Eaton (2010), Turbulent dispersed multiphase flow, *Annual Review of Fluid Mechanics*, *42*, 111–133.

Benavides, A., and B. van Wachem (2008), Numerical simulation and validation of dilute turbulent gasparticle flow with inelastic collisions and turbulence modulation, *Powder Technology*, *182*(2), 294–306.

Calantoni, J., and J. A. Puleo (2006), Role of pressure gradients in sheet flow of coarse sediments under sawtooth waves, *Journal of Geophysical Research: Oceans (19782012)*, *111*(C1).

Carnahan, N. F., and K. E. Starling (1969), Equation of state for nonattracting rigid spheres, *The Journal of Chemical Physics*, *51*(2), 635–636.

Chapman, S., and T. G. Cowling (1970), *The mathematical theory of non-uniform gases: an account of the kinetic theory of viscosity, thermal conduction and diffusion in gases*, Cambridge university press.

Chen, C. P., and P. E. Wood (1985), A turbulence closure model for dilute gas-particle flows, *Can. J. Chem. Eng.*, *63*(3), 349–360.

Chen, J.-L., F. Shi, T.-J. Hsu, and J. T. Kirby (2014), Nearcom-tvd–quasi-3d nearshore circulation and sediment transport model, *Coastal Engineering*, *91*, 200–212.

Chen, X., Y. Li, X. Niu, D. Chen, and X. Yu (2011), A two-phase approach to wave-induced sediment transport under sheet flow conditions, *Coastal Engineering*, *58*(11), 1072–1088.

Chou, Y.-J., and O. B. Fringer (2010), A model for the simulation of coupled flow-bed form evolution in turbulent flows, *J. Geophys. Res.*, *115*(C10), C10,041.

Danon, H., M. Wolfshtein, and G. Hetsroni (1977), Numerical calculations of two-phase turbulent round jet, *International Journal of Multiphase Flow*, *3*(3), 223–234.

Ding, J., and D. Gidaspow (1990), A bubbling fluidization model using kinetic theory of granular flow, *AIChE J.*, *36*(4), 523–538.

Dong, P., and K. Zhang (1999), Two-phase flow modelling of sediment motions in oscillatory sheet flow, *Coastal Engineering*, *36*(2), 87–109.

Dong, P., and K. Zhang (2002), Intense near-bed sediment motions in waves and currents, *Coastal Engineering*, *45*(2), 75–87.

Drake, T. G., and J. Calantoni (2001), Discrete particle model for sheet flow sediment transport in the nearshore, *Journal of Geophysical Research: Oceans (19782012)*, *106*(C9), 19,859–19,868.

Drew, D. A. (1983), Mathematical modeling of two-phase flow, *Annual review of fluid mechanics*, *15*(1), 261–291.

Engelund, F., and J. Fredsoe (1976), A sediment transport model for straight alluvial channels, *Nordic Hydrology*, *7*(5), 293–306.

Ergun, S. (1952), Fluid flow through packed columns, *Chem. Eng. Prog.*, *48*, 89–94.

Gidaspow, D. (1994), *Multiphase flow and fluidization: continuum and kinetic theory descriptions*, Academic press.

Higuera, P., J. L. Lara, and I. J. Losada (2013), Simulating coastal engineering processes with openfoam, *Coastal Engineering*, *71*, 119–134.

Hsu, T.-J., and D. M. Hanes (2004), Effects of wave shape on sheet flow sediment transport, *Journal of Geophysical Research: Oceans (1978-2012)*, *109*(C5).

Hsu, T.-J., J. T. Jenkins, and P. L. Liu (2003), On two-phase sediment transport: Dilute flow, *Journal of Geophysical Research: Oceans (1978-2012)*, *108*(C3).

Hsu, T.-J., J. T. Jenkins, and P. L.-F. Liu (2004), On two-phase sediment transport: sheet flow of massive particles, *Proceedings of the Royal Society of London. Series A: Mathematical, Physical and Engineering Sciences*, *460*(2048), 2223–2250.

Jacobsen, N. G., D. R. Fuhrman, and J. Fredse (2012), A wave generation toolbox for the open-source cfd library: Openfoam, *Int. J. Numer. Meth. Fluids*, *70*(9), 1073–1088.

Jenkins, J., and S. Savage (1983), A theory for the rapid flow of identical, smooth, nearly elastic, spherical particles, *Journal of Fluid Mechanics*, *130*, 187–202.

Johnson, P. C., and R. Jackson (1987), Frictional-collisional constitutive relations for granular materials, with application to plane shearing, *Journal of Fluid Mechanics*, *176*, 67–93.

Kranenburg, W. M., T.-J. Hsu, and J. S. Ribberink (2014), Two-phase modeling of sheet-flow beneath waves and its dependence on grain size and streaming, *Advances in Water Resources*.

Lesser, G., J. Roelvink, J. van Kester, and G. Stelling (2004), Development and validation of a three-dimensional morphological model, *Coastal Engineering*, *51*(89), 883–915.

Li, M., S. Pan, and B. A. O'Connor (2008), A two-phase numerical model for sediment transport prediction under oscillatory sheet flows, *Coastal Engineering*, *55*(12), 1159–1173.

Liu, H., and S. Sato (2006), A two-phase flow model for asymmetric sheetflow conditions, *Coastal Engineering*, *53*(10), 825–843.

Liu, X., and M. Garcia (2008), Three-dimensional numerical model with free water surface and mesh deformation for local sediment scour, *J. Waterway, Port, Coastal, Ocean Eng.*, *134*(4), 203–217, doi:10.1061/(ASCE)0733-950X(2008)134:4(203).

Lun, C. K. K., S. B. Savage, D. J. Jeffrey, and N. Chepurniy (1984), Kinetic theories for granular flow: inelastic particles in couette flow and slightly inelastic particles in a general flowfield, *Journal of Fluid Mechanics*, *140*, 223–256 M3 – 10.1017/S0022112084000,586.

Marieu, V., P. Bonneton, D. L. Foster, and F. Ardhuin (2008), Modeling of vortex ripple morphodynamics, *J. Geophys. Res.*, *113*(C9), C09,007.

Maxey, M. R., and J. J. Riley (1983), Equation of motion for a small rigid sphere in a nonuniform flow, *Physics of Fluids (1958-1988)*, *26*(4), 883–889, doi: http://dx.doi.org/10.1063/1.864230.

McTigue, D. F. (1981), Mixture theory for suspended sediment transport, *Journal of the Hydraulics Division*, *107*(6), 659–673.

O'Donoghue, T., and S. Wright (2004), Concentrations in oscillatory sheet flow for well sorted and graded sands, *Coastal Engineering*, *50*(3), 117–138.

Ozdemir, C. E., T.-J. Hsu, and S. Balachandar (2010), A numerical investigation of fine particle laden flow in an oscillatory channel: the role of particle-induced density stratification, *Journal of Fluid Mechanics*, *665*, 1–45 M3 – 10.1017/S0022112010003,769.

Peltola, J. (2009), Dynamics in a circulating fluidized bed: Experimental and numerical study, Master's thesis, Tampere University of Technology.

Penko, A. M., D. N. Slinn, and J. Calantoni (2010), Model for mixture theory simulation of vortex sand ripple dynamics, *Journal of Waterway, Port, Coastal, and Ocean Engineering*, *137*(5), 225–233.

Rhie, C., and W. Chow (1983), Numerical study of the turbulent flow past an airfoil with trailing edge separation, *AIAA journal*, *21*(11), 1525–1532.

Ribberink, J. S. (1998), Bed-load transport for steady flows and unsteady oscillatory flows, *Coastal Engineering*, *34*(12), 59–82.

Rusche, H. (2002), Computational fluid dynamics of dispersed two-phase flows at high phase fractions, Ph.D. thesis, Imperial College London (University of London).

Schaeffer, D. G. (1987), Instability in the evolution equations describing incompressible granular flow, *Journal of differential equations*, *66*(1), 19–50.

Scott, N. V., T.-J. Hsu, and D. Cox (2009), Steep wave, turbulence, and sediment concentration statistics beneath a breaking wave field and their implications for sediment transport, *Continental Shelf Research*, *29*(20), 2303–2317.

Sinclair, J., and R. Jackson (1989), Gasparticle flow in a vertical pipe with particle-particle interactions, *AIChE Journal*, *35*(9), 1473–1486.

Srivastava, A., and S. Sundaresan (2003), Analysis of a frictional-kinetic model for gas-particle flow, *Powder technology*, *129*(1), 72–85.

Sumer, B. M., A. Kozakiewicz, J. Fredse, and R. Deigaard (1996), Velocity and concentration profiles in sheet-flow layer of movable bed, *Journal of Hydraulic Engineering*, *122*(10), 549–558.

Tardos, G. I. (1997), A fluid mechanistic approach to slow, frictional flow of powders, *Powder Technology*, *92*(1), 61–74.

van Rijn, L. C. (1984), Sediment pick-up functions, *Journal of Hydraulic Engineering*, *110*(10), 1494–1502.

Warner, J. C., C. R. Sherwood, R. P. Signell, C. K. Harris, and H. G. Arango (2008), Development of a three-dimensional, regional, coupled wave, current, and sediment-transport model, *Computers & Geosciences*, *34*(10), 1284–1306.

Weller, H. (2002), Derivation, modelling and solution of the conditionally averaged two-phase flow equations, *Tech. rep.*, OpenCFD Ltd.

Wen, C., and Y. Yu (1966), Mechanics of fluidization, in *Chem. Eng. Prog. Symp. Ser.*, vol. 62, p. 100.

Yu, X., T.-J. Hsu, and D. M. Hanes (2010), Sediment transport under wave groups: Relative importance between nonlinear waveshape and nonlinear boundary layer streaming, *Journal of Geophysical Research: Oceans (1978-2012)*, *115*(C2).

Yu, X., T.-J. Hsu, J. T. Jenkins, and P. L.-F. Liu (2012), Predictions of vertical sediment flux in oscillatory flows using a two-phase, sheet-flow model, *Advances in Water Resources*, *48*(0), 2–17.